American Scientific Research Journal for Engineering, Technology, and Sciences (ASRJETS)
ISSN (Print) 2313-4410, ISSN (Online) 2313-4402

http://asrjetsjournal.org/

Static Analysis of a Rotating Part

Mustafa Sulaiman AL-Nabhani[a], Rui Cai[b]*

[a,b]*Department of Mechanical Engineering, Coventry University , Priory Street, Coventry CV1 5FB, United Kingdom*

[a]*Email: mustafas.soh@cas.edu.om*

[b]*Email: ab9225@coventry.ac.uk*

Abstract

In this study, the composite orthotropic annular rotating part of carbon fibre reinforced polymer is investigated statically. Rotating structure is modeled in CATIA V5 and meshed in HyperMesh 13.0 to be analytically simulated in ANSYS 16.1 APDL. The static behaviour of the radial, circumferential and longitudinal stresses and deformations are obtained and analysed at six various angular velocities up to 2727.27 rad/s. It is noted that the simulated magnitudes of the hoop stress are higher than that of the radial and longitudinal stresses. However, the maximum displacements are found to be in the longitudinal and radial directions respectively. In addition, these stresses are observed to increase as the angular velocities increased.

Keywords: Composite material; FEA; Rotating part; Stress analysis.

1. Introduction

Carbon fibre reinforced polymer is one of the most advanced composite materials that is being increasingly used in various engineering industrial applications, such as the automotive, marine and aerospace industries [1]. The main advantages or a characteristic of CFRP is its flexibility in relation to design, high resistivity to corrosion, plus, its high strength and stiffness [1]. Therefore, this material is commonly used in turbines, generators, engines and compressors. In most structural and industrial applications related to CFRP, it has been observed that this material is subjected to long term cyclic loading and unloading conditions of variable and excessive stresses and strains that indicate that CFRP is likely to fail at a specific number of cycles [1]. In addition, the authors in [2] suggested that the rotating structures found on these applications are subjected to high rotational speeds that can induce high centrifugal force.

---

* Corresponding author.

The authors in [2] further proposed that the maximum rotating stresses generated due to centrifugal force should be considered in the design. Investigating the static behaviour of the composite rotating part is necessary to determine the fatigue behaviour which is expected to occur at a certain limit in relation to the rotational speed. The static behaviour is investigated on the maximum location of the cyclic stresses and deformations that may cause various failure modes on the rotating part. The authors in [3] indicated that there are three alternative stresses acting on the rotating parts: radial, circumferential and longitudinal stresses. Therefore, the authors in [2] corroborated that the variation of these stresses with respect to rotational speeds should be investigated. Numerous published papers studied the static behaviour of various applications of the rotating parts under different conditions of loads, pressures, temperatures and constraints. However, this paper is only used to analyse the theoretical and simulated static behaviour of a section of the full rotating part under different angular velocities up to 600 m/s to predict and investigate the static behaviour of the adopted rotating structure.

2. Literature Review

Static analysis is a subset of structural analysis which is used to determine the stresses, strains, displacements and reactional forces induced by static loading conditions subjected to the structures or components [4]. However, the damping and inertial effects which are caused by time varying loading conditions are neglected [4]. The static loading types that can be considered and applied to the components include the external forces, pressures, temperature and inertial forces generated because of gravity and rotational speeds [4]. The authors in [3] investigated that there are three alternative stresses acting on the rotating parts: axial, hoop and radial stresses. The authors in [3] also noted that the axial or what is known as longitudinal stress is stress that acts along the axial direction of an object. While the hoop stress or what is termed circumferential stress is defined as the stress that acts along the perpendicular direction to the radial stress. However, the radial stress is the stress that acts along the radial direction of the object [3]. The authors in [3,5] analysed and investigated the behaviour of the most common types of rotating parts, such as thin, solid, hollow and thick discs. The author in [5] additionally advocated that the general equation of centrifugal force that can be used for the most common types of rotating parts is expressed as shown in Equation (1).

$$F=m\times a=m\ \omega^2 r^2 \qquad (1)$$

Where the general equations that can be used to determine the hoop and radial stresses at any radius of the uniform thickness and constant angular velocity of the rotating parts can be expressed as shown in Equations (2) and (3) respectively [5]:

$$\sigma_H=A+\frac{B}{r^2}-(1+3v)\frac{\rho\omega^2 r^2}{8} \qquad (2)$$

$$\sigma_r=A-\frac{B}{r^2}-(3+v)\frac{\rho\omega^2 r^2}{8} \qquad (3)$$

The author in [5] studied that the hoop and radial stresses equations that can be used for the rotating part with a central hole can be obtained by using the following two equations respectively.

$$\sigma_H=\frac{\rho\omega^2}{8}\left[\ (3+v)\ \left(R_1^2+R_2^2+\frac{R_1^2R_2^2}{r^2}\right)-(1+3v)r^2\right] \qquad (4)$$

$$\sigma_r=(3+v)\frac{\rho\omega^2}{8}\left[\ R_1^2+R_2^2-\frac{R_1^2R_2^2}{r^2}-r^2\right] \qquad (5)$$

The author in [5] also observed that the maximum hoop stress for this type can be determined at the inside radius, where $r = R_1$, as shown in Equation (6).

$$\sigma_{Hmax}=\frac{\rho\omega^2}{4}\left[\ (3+v)R_2^2+(1-v)\ R_1^2\right] \qquad (6)$$

However, the author in [5] reported that when the inside radius approaches zero, the peak hoop stress can be obtained, as determined in Equation (7).

$$\sigma_{H\,max}=\frac{\rho\omega^2}{4}\left[\ (3+v)R_2^2\right] \qquad (7)$$

Conversely, the minimum hoop stress can be determined at $r = R_2$, where the radius of any section equals to the outside radius of the rotating part, as obtained in Equation (8) [5].

$$\sigma_{H\,min}=\frac{\rho\omega^2}{4}\left[\ (3+v)R_1^2+(1-v)\ R_2^2\right] \qquad (8)$$

While the maximum radial stress can be determined at the radius where $r = \sqrt{R_1R_2}$ which is derived from Equation (5) at $\frac{d\sigma_r}{dr} = 0$ to obtain the maximum value of the radial stress by using the theorem of the first derivative, as shown in Equation (9) [5].

$$\sigma_{r_{max}}= (3+v)\frac{\rho\omega^2}{8}\ [\ R_2-R_1]^2 \qquad (9)$$

Furthermore, the author in [5] indicated that the maximum hoop and radial stresses for a small hollow disc can be expressed, as revealed in Equations (10) and (11) respectively.

$$\sigma_{H\,max}=\frac{\rho\omega^2}{4}\left[\ (3+v)R_2^2\right] \qquad (10)$$

$$\sigma_{r_{max}}= (3+v)\frac{\rho\omega^2}{8}\ [\ R_2]^2 \qquad (11)$$

However, the authors in [6] implied that the hoop and radial stresses generated by rotational speeds can be expressed and subjected under gravitational acceleration, as described in Equations (12) and (13) respectively.

$$\sigma_{H\,max} = \frac{\rho\omega^2}{4g}\left[\ (3+v)R_2^2\right] \qquad (12)$$

$$\sigma_{r_{max}} = (3+v)\frac{\rho\omega^2}{8g}\left[\ R_2\right]^2 \qquad (13)$$

The author in [5] additionally demonstrated the distribution of the hoop and radial stresses over this type, as shown in Figure 1.

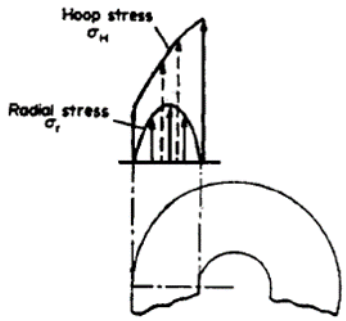

Figure 1: Distribution of hoop and radial stresses over the rotating part of a central hole [5]

3. Research Methodology

3.1 Modeling Method

CATIA V5 software is used to construct the model of the rotating part. This software is predominantly used by many industrial engineers and designers for 3D models and 2D sketches [7]. In addition, this software is utilised by various industrial sectors, such as the aerospace and automotive industries (Reddy and Kumar 2015). The design concept of the designed structure is shown in Figure 2 below.

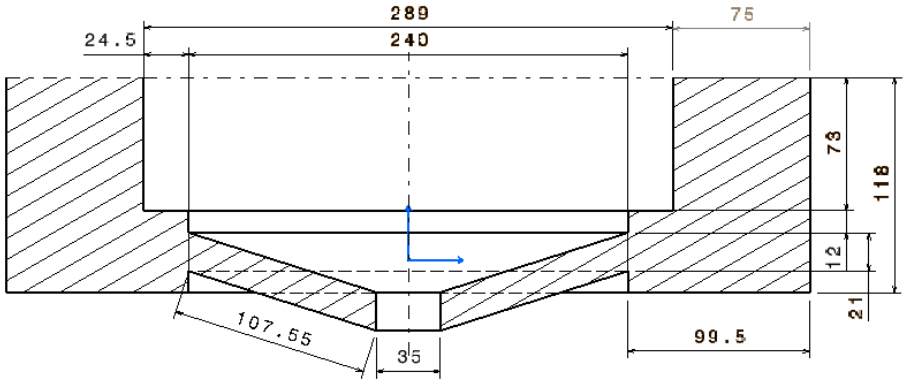

Figure 2: 2D-Sketch of the rotating part

However, a section of a 45° rotating part is adopted and modeled in CATIA V5, as illustrated in Figure 3. This section is selected to avoid the maximum limit of nodes specified or allowed in the academic educational version.

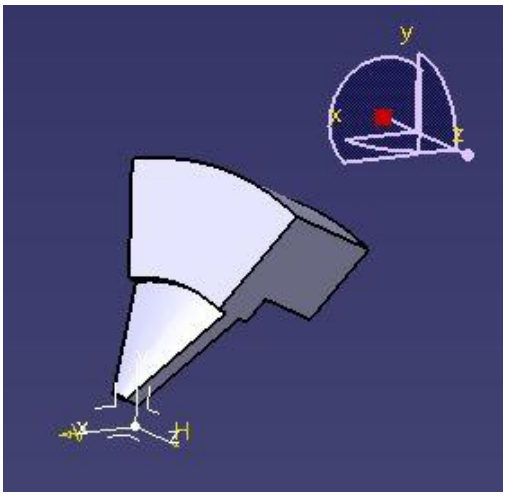

Figure 3: 45° section of the full rotating part

Consequently, Figure 4 illustrates the full dimensions of the modeled rotating section from different sides, sketched in a CATIA V5 Drafting worksheet.

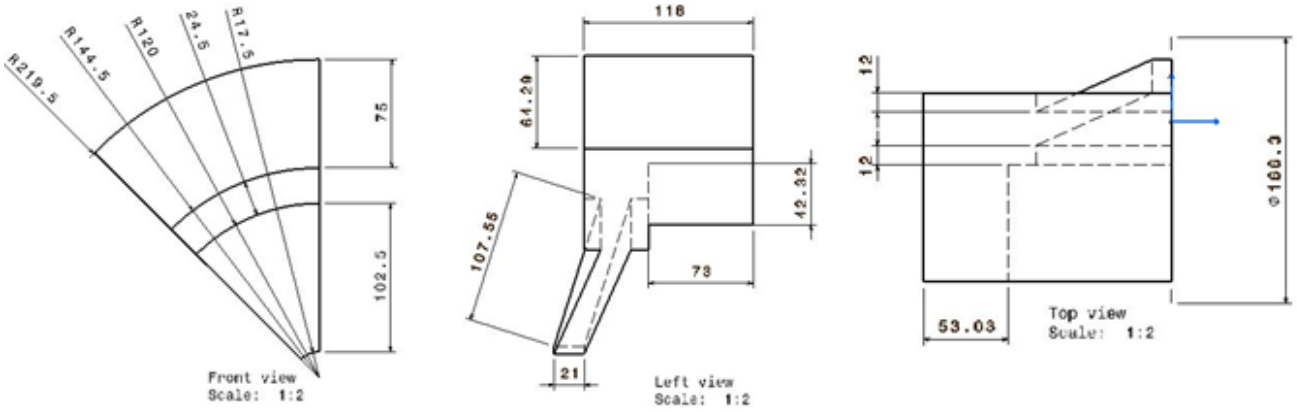

Figure 4: Different sides of views of 45° section of the rotating part

Table 1: Parametres of modelled rotating structure

Parameters	Value
Mass	2.29 Kg
Volume	1.419×10^{6} mm^3
Disc diameter	439 mm
Shaft diameter	35 mm
Angle	45°

Table 1 shows several structural parameters of the modeled geometry.

3.2 Meshing Method

Hyper Mesh 13.0 software is selected and performed to mesh the designed structure. The meshing tool of the solid mapping mesh is selected and applied to mesh the rotating structure by choosing the meshing style of the squared element shape, as shown in Figure 5. This meshing tool is constructed by splitting and meshing three different faces of the rotating structure by using a 2D auto-mesh tool with a 4mm meshing size. Subsequently, this 2D mesh is extended and dragged along the line vector through the solid volume with a 1mm meshing size.

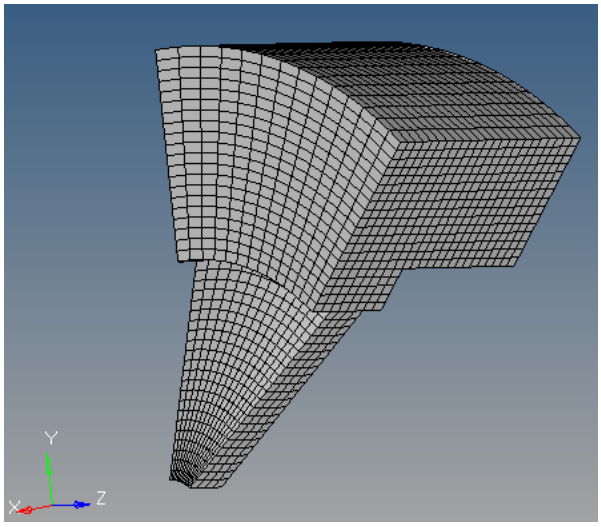

Figure 5: Meshing of the rotating part

3.3 FEA Method

The finite element analysis software is adopted to analyse the present structure of the rotating part is the Mechanical Structural Analysis (APDL) of ANSYS 16.1. This software is employed to investigate the static behaviour of the rotating section under different cases of angular velocities. Consequently, the structural behaviour of this rotating section is analysed in ANSYS APDL 16.1 by applying several steps Figure 6 envisages the schematic flowchart of the common development process performed in the FEA-model to obtain the static structural analysis of the rotating section

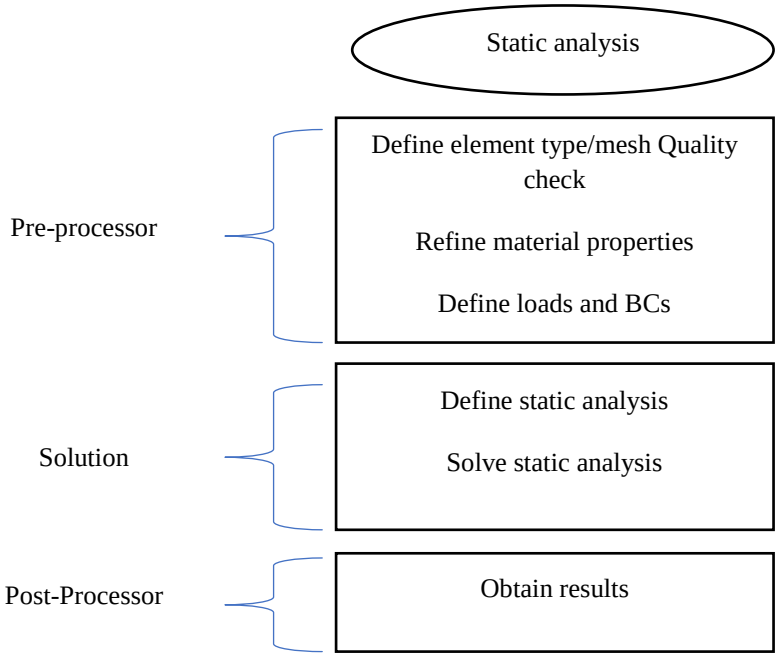

Figure 6: Schematic representation of the development process of the static FE-model

3.4 Material properties and element type

The material properties of the carbon fibre reinforced polymer are adopted in the present analysis. Table 2 shows several mechanical and thermal properties of CFRP.

Table 2: Material properties of CFRP [8]

CFRP- Max speed 600 m/s, Density of 1620 Kg/m^3						
T(□)	E_{xx}(MPa)	E_{yy}(MPa)	E_{zz}(MPa)	v_{xy}	v_{yz}	v_{xz}
-40	7787	189403	7787	0.01	0.01	0.358
T(□)	G_{xy}(MPa)	G_{yz}(MPa)	G_{xz}(MPa)	$\alpha_{xx}(10^{-6})/$□	$\alpha_{yy}(10^{-6})/$□	$\alpha_{zz}(10^{-6})/$□
-40	4826	4878	4070	27.5	-0.299	27.1

However, Table 3 reveals the element type of the rotating structure, in addition to its number of nodes and elements obtained from the Hyper Mesh 13.0.

Table 3: Element specifications of the rotating section

Element type	Solid 185
Elements	9730
Nodes	11655

3.5 Boundary condition and load

The boundary conditions and the load applied to the rotating structure to obtain the static structural analysis is shown in Figure 7. It can be clearly seen that both sides of the rotating structure are constrained in the circumferential direction of the Y-axis. In addition, the directional axes of X, Y and Z are fully constrained at the centre of the rotating structure. The inertia load of the rotational speed, conversely, is applied at the centre of the rotating part.

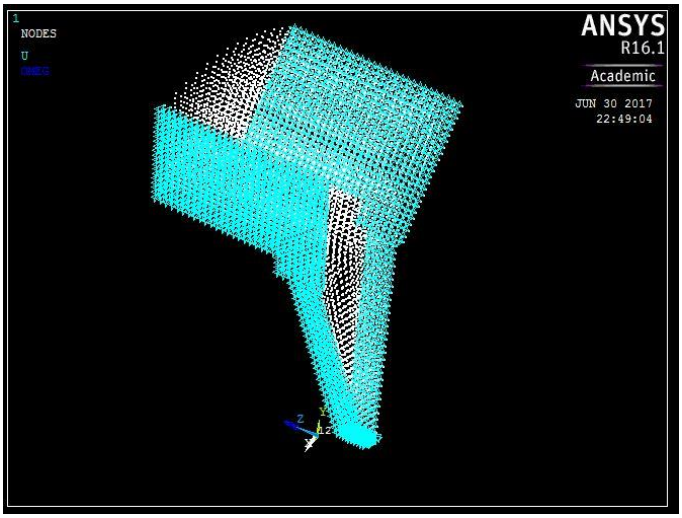

Figure 7: BCs applied to the rotating section

4. Results and Discussion

The static finite element analysis model is used to demonstrate and discuss the results of the maximum stresses and deformations of the cylindrical coordinate system acting on the rotating structure when this rotating mass is subjected to different angular velocities and specific boundary conditions. In the static structural analysis, sufficient boundary conditions are applied to the rotating part, specifically in the Z-axis and Y-axis to prevent the free translating motion along the longitudinal direction of the cylindrical coordinate system in addition to preventing the free rotating motion that could possibly occur around the circumferential direction of the cylindrical coordinate system.

4.1 Results of the directional stresses

The contour plots of the maximum and minimum radial stresses, hoop stresses and longitudinal stresses generated due to the maximum angular speed of 2727.27 rad/s are shown in Figures 8, 9 and 10 respectively. The distribution of these stresses is investigated when the rotating mass spins around the Z-axis.

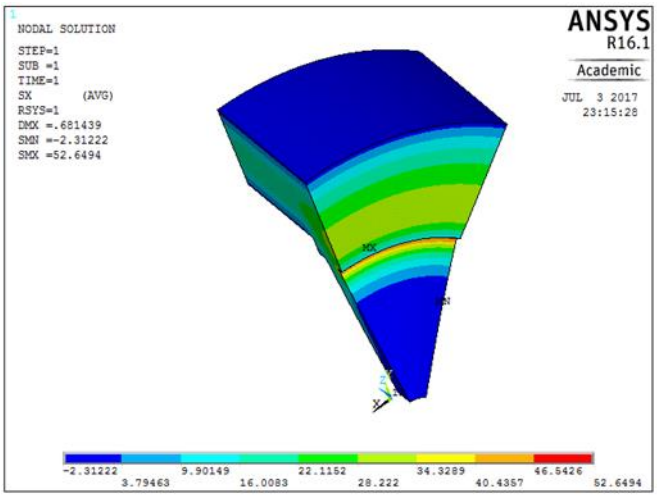

Figure 8: The contour plot of maximum and minimum radial stresses generated due to 2727.27 rad/s

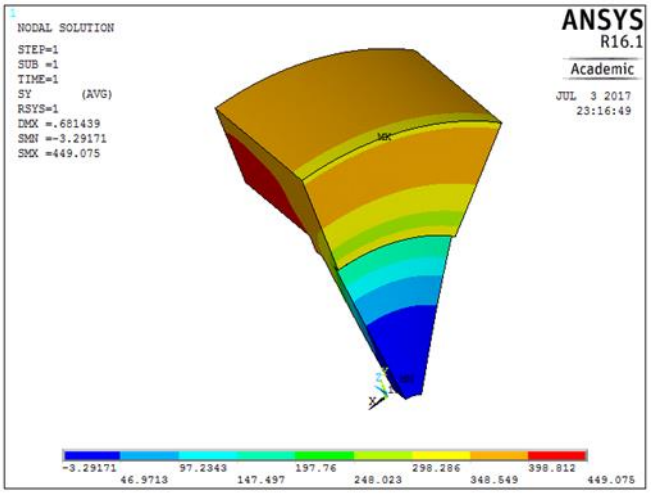

Figure 9: The contour plot of maximum and minimum hoop stresses generated due to 2727.27 rad/s

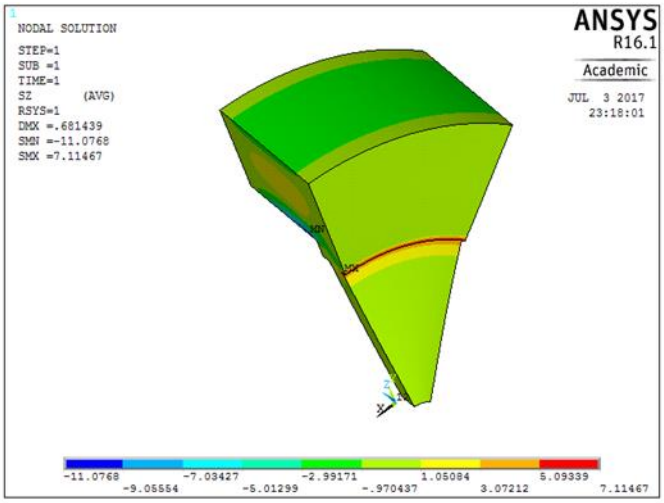

Figure 10: The contour plot of maximum and minimum longitudinal stresses generated due to 2727.27 rad/s

It can be clearly observed from Figures 8, 9 and 10 that the location of the maximum radial stress is found to be at the centre of the composite rotating structure, which is induced because of the high rotational speed of 26043.5 rpm. While the maximum hoop or circumferential stress is determined to be along the rotational direction, which is closed to the outer radius. However, the maximum longitudinal stress of the simulated structure is found to be in the middle of the rotating structure due to central rotational speed applied to the structure and change in thickness of the rotating structure. This rotating section is performed under six various angular velocities. Therefore, Table 4 demonstrates the maximum radial, hoop and longitudinal stresses of each velocity obtained from ANSYS 16.1.

Table 4: The maximum cylindrical stresses generated due to different angular speeds

ω(rad/s)	$\sigma_{r,max}$(MPa)	$\sigma_{H,max}$(MPa)	$\sigma_{L,max}$(MPa)
454.55	1.46	12.47	0.31
909.09	5.85	49.90	1.23
1363.64	13.16	112.27	2.77
1818.18	23.40	199.59	4.92
2272.73	36.56	311.86	7.69
2727.27	52.65	449.08	11.10

It can be clearly seen from Table 4 above that the maximum stresses generated due to different cases of the angular velocities are found to be in the hoop direction, which indicates that the hoop stress is the dominant stress on the rotating structure. The minimum stresses, in contrast, are found to be in the longitudinal direction.

4.2 Results of Von Misses stresses

The contour plot of the Von Misses stresses generated by the maximum angular speed of 2727.27 rad/s is depicted in Figure 11

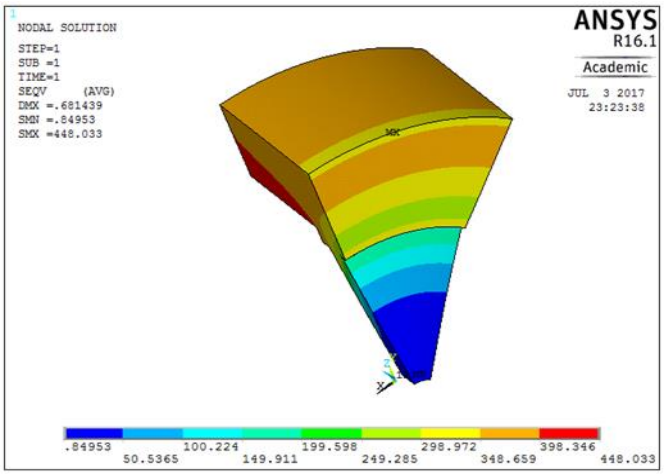

Figure 11: The contour plot of maximum and minimum Von Misses stresses generated by 2727.27 rad/s

The simulated results of the Von Misses stresses can be theoretically validated and calculated by using the general equation of the Von Misses criteria, as expressed in Equation (14) below (Lawrence and Ya 2014) .

$$\sigma_{Von\ Misses}=\sqrt{\sigma_{r,max}{}^2-\sigma_{r,max}\sigma_{H,max}+\sigma_{H,max}{}^2} \qquad (14)$$

The authors in [9] implied that the ultimate strength of the CFRP sheet is equal to 3553 MPa. Therefore, the stress induced due to the angular velocities should be less than this amount to avoid the failure modes. It can be clearly observed from the above figure that the maximum equivalent stress generated by the maximum rotational speed does not exceed the ultimate allowable stress related to CFRP. This action indicates that this structure can operate safely under different velocities without failing. Furthermore, the authors in [10] indicated that the factor of safety for composites can be mathematically calculated by dividing the ultimate stress of the CFRP material to the maximum actual stress induced due to the rotational speeds, as expressed in Equation (15).

$$F.O.S=\frac{\sigma_{ultimate}}{\sigma_{actual}} \qquad (15)$$

Therefore, Table 5 shows the theoretical calculations of the factor of safety related to CFRP for each angular velocity of 454.55 rad/s, 909.09 rad/s, 1363.64 rad/s, 1818.18 rad/s, 2272.73 rad/s and 2727.27 rad/s respectively.

Table 5: Factor of safety calculations

ω(rad/s)	$\sigma_{ultimate}$(MPa)	$\sigma_{Von\ Misses,max}$(MPa)	F.O.S	Status
454.55	3553	12.45	285.38	Safe
909.09	3553	49.78	71.37	Safe
1363.64	3553	112.01	31.72	Safe
1818.18	3553	199.13	17.84	Safe
2272.73	3553	311.14	11.42	Safe
2727.27	3553	448.03	7.93	Safe

4.3 Results of the directional deformation

Figures 12, 13 and 14 illustrate the contour plots of the maximum deformations that occur in the X-direction (radial), Y-direction (circumferential or hoop) and Z-direction (longitudinal), which is simulated when the rotating section revolves around the Z-direction at the maximum angular velocity of 2727.27 rad/s.

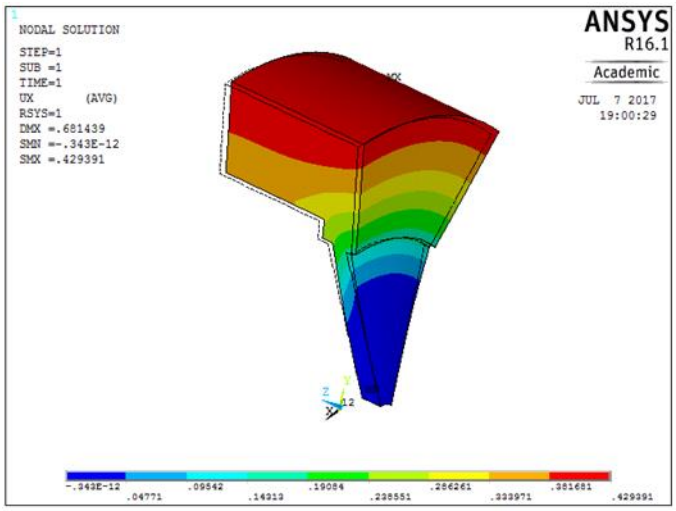

Figure 12: The contour plot of the maximum radial deformation induced due to 2727.27 rad/s

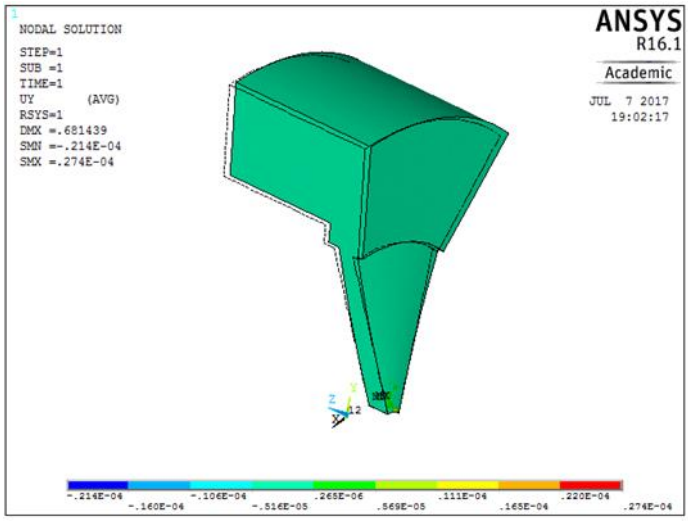

Figure 13: The contour plot of the maximum hoop deformation induced due to 2727.27 rad/s

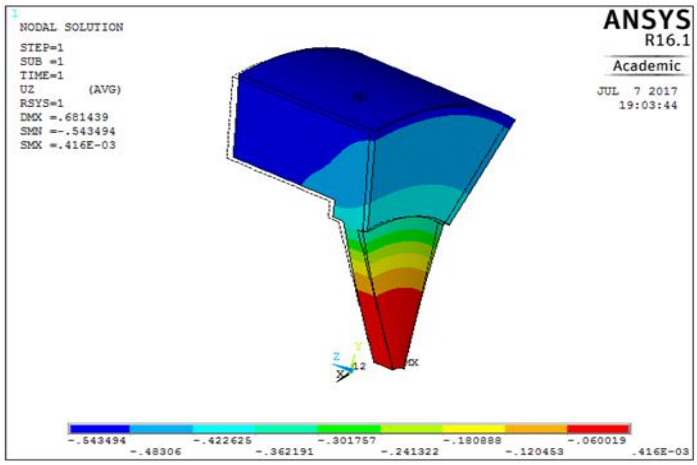

Figure 14: The contour plot of the maximum longitudinal deformation induced due to 2727.27 rad/s

It can be clearly noted from Figure 12 that the maximum deformation of the radial direction is located at the outer side of the rotating structure, as visualised in red. In addition, the longitudinal deformation is also located in the outer zone of the rotating structure as visualised in blue, as shown in Figure 14 above. However, the circumferential deformation is exceedingly small compared to the previous deformations and it is uniformly distributed along the entire shape of the rotating component, as demonstrated in Figure 13 above. Moreover, Table 5 shows the maximum deformations along the radial, hoop and longitudinal directions of the cylindrical coordinate axes, induced by the angular velocities of 454.55 rad/s, 909.09 rad/s, 1363.64 rad/s, 1818.18 rad/s, 2272.73 rad/s and 2727.27 rad/s.

Table 5: Summary of directional deformation results

ω(rad/s)	U_x(mm)	U_y(mm)	U_z(mm)
454.55	0.012	0.76×10^{-6}	0.015
909.09	0.048	0.30×10^{-5}	0.06
1363.64	0.11	0.69×10^{-5}	0.14
1818.18	0.19	0.12×10^{-4}	0.24
2272.73	0.30	0.19×10^{-4}	0.38
2727.27	0.43	0.27×10^{-4}	0.54

It can be determined from Table 5 above that maximum deformation is found to occur in the longitudinal and radial directions respectively. The longitudinal deformation occurs due to the translational motion of the rotating structure when the structure is subjected to high rotational speed around the Z-axis. The radial deformation occurs due to the extremely low radial strength of the composite rotating structure which could lead to the delamination failure mode. However, the minimum deformation is observed to be in the hoop or circumferential direction because of the boundary conditions used to restrain or prevent the higher displacements in the Y-axis.

5. Conclusion

In conclusion, this paper investigated the static behaviour of a composite rotating part. The orthotropic material properties of carbon fibre reinforced polymer are adopted in the theoretical and analytical solutions. A section of 45° rotating part is established and constructed in CATIA V5. Subsequently, Hyper Mesh 13.0 is adopted to discretise this structure into 11655 nodes and 9730 elements to be statically analysed in ANSYS 16.1 at different angular velocities. The maximum static analysis of the radial, hoop and longitudinal stresses and deformations induced due to the maximum angular speed of 2727.27 rad/s are obtained and analysed. It was observed that the magnitudes of the hoop stress are higher than that of the radial and longitudinal stresses. Nevertheless, maximum deformations are found to be in the longitudinal and radial directions compared to the circumferential direction.

References

[1]. A. Amiri, M. Cavalli and C. Ulven, "A new approach of stiffness degradation modeling for carbon fiber-reinforced polymers under cyclic fully reversed bending", Journal of Composite Materials, vol. 51, no. 20, pp. 2889-2897, 2017.

[2]. V. Belyaev, A. Zurilin and S. Cherkasov, "On the Strength Calculation of the Rotating parts", Procedia Chemistry, vol. 10, pp. 151-157, 2014.

[3]. M. Shariyat and R. Mohammadjani, "Three-dimensional compatible finite element stress analysis of spinning two-directional FGM annular plates and disks with load and elastic foundation non-uniformities", Latin American Journal of Solids and Structures, vol. 10, no. 5, pp. 859-890, 2013.

[4]. E. Dill, The finite element method for mechanics of solids with ANSYS applications. Boca Raton, Fla.: CRC Press, 2012.

[5]. E. Hearn, An introduction to the mechanics of elastic and plastic deformation of solids and structural materials.3 rd ed. Oxford: Butterworth-Heinemann, 1997.

[6]. K. Kobia, and Y. Mao, " Finite Element Analysis of Radial Stress Distribution on Axisymmetric Variable Thickness Dual Mass Flywheel Using ANSYS ", Innovative Systems Design and Engineering, vol. 5, pp. 44-50, 2014.

[7]. K. Reddy, and B. Kumar, " Design And Analysis Of Flywheel By Using Finite Element Analysis ", International Journal Of Emerging Technologies In Engineering Research (IJETER), vol. 3, pp. 40-46, 2015.

[8]. R. Cai, "Material Properties of Carbon Fiber reinforced Polymer", Coventry University, 2017.

[9]. Y. Lu, W. Li, S. Li, X. Li and T. Zhu, "Study of the Tensile Properties of CFRP Strengthened Steel Plates", Polymers, vol. 7, no. 12, pp. 2595-2610, 2015.

[10]. R. Khurmi and J. Gupta, A textbook of machine design, 1st ed. New Delhi: Eurasia Publishing House, 2005.